

Artificial Neural Network (FFBP-ANN) Based Grey Relational Analysis for Modeling Dyestuff Solubility in Supercritical CO₂ with Ethanol as the Co-Solvent

Srinidhi,^{1,*} Deepak Patel,² Vasantha Kumara S. A.,^{3,*}

¹ Department of Biotechnology Engineering, Ramaiah Institute of Technology, Bangalore, Karnataka, India.

² Department of Mechanical Engineering, Global Institute of Technology, Bangalore, Karnataka, India.

³ Professor and Head, Department of Industrial Engineering and Management, Dayananda Sagar College of Engineering, Bangalore, Karnataka, India.

Correspondence: msrinidhi2@gmail.com , vasanthakumara-iem@dayanandasagar.edu

1 Abstract

The research on dye solubility modeling in supercritical carbon dioxide is gaining prominence over the past few decades. A simple and ubiquitous model that is capable of accurately predicting the solubility in supercritical carbon dioxide would be invaluable for industrial and research applications. In this study, we present such a model for predicting dye solubility in supercritical carbon dioxide with ethanol as the co-solvent for a qualitatively diverse sample of eight dyes. A feed forward back propagation - artificial neural network model based on Levenberg-Marquardt algorithm was constructed with seven input parameters for solubility prediction, the network architecture was optimized to be [7-7-1] with mean absolute error, mean square error, root mean square error and Nash-Sutcliffe coefficient to be 0.026, 0.0016, 0.04 and 0.9588 respectively. Further, Pearson-product moment correlation analysis was performed to assess the relative importance of the parameters considered in the ANN model. A total of twelve prevalent semi-empirical equations were also studied to analyze their efficiency in correlating to the solubility of the prepared sample. Mendez-Teja model was found to be relatively efficient with root mean square error and mean absolute error to be 0.094 and 0.0088 respectively. Furthermore, Grey relational analysis was performed and the optimum regime of temperature and pressure were identified with dye solubility as the higher the better performance characteristic. Finally, the dye specific crossover ranges were identified by analysis of isotherms and a strategy for class specific selective dye extraction using supercritical CO₂ extraction process is proposed.

Keywords: artificial neural network modeling, supercritical fluid extraction, Grey relational analysis, Dyestuff solubility.

2 Introduction

Supercritical fluid extraction has been amassing prominence as an effective method to separate and purify a variety of substances from multi-component mixtures. Supercritical fluid extraction has been employed for the purification of a raft of different products ranging from petrochemicals [1] to phytochemicals [2] and from dyes [3] to radioactive elements [4]. Among the different solvents employed in the supercritical fluid extraction process, CO₂ has been extensively used for many of its fitting and desirable attributes [5]. The diversity of product applications of supercritical

CO₂ extraction calls for the need to model the process accurately. Experimentation of supercritical fluid extraction on high-value dyestuff just for the sake of modeling is resource consuming and costly. Therefore, research focused on modeling the solubility of dyestuff using supercritical fluid extraction process using empirical data is being pursued at an accelerating pace over the past few decades. Although cubic equations of state are widely used to calculate solubilities of solutes in supercritical CO₂, they are highly disadvantageous for application in industries for the various reasons explained by Gharagheizi et al [6]. Further, Semi-empirical models, models involving mass transfer phenomenon, and Black box approaches like wavelet neural network modeling, artificial neural networks, Fuzzy logic technology, Response surface methodology, have also been studied for general solubility modeling purposes for the supercritical CO₂ extraction process. Black-box modeling strategies are beneficial in modeling processes as they are devoid of tedious theoretical mathematical modeling and are industry-friendly approaches [7].

Artificial neural network simulation is one such black-box approach that is showing promise for tackling multivariate and complex modeling problems. Artificial neural networks and other machine learning algorithms are employed for their high sensitivity to change in variables, accommodation for a large number of variables, flexibility, ease in network construction, and the diverse availability of adjustable functions for precision modeling and prediction [8]. Prominently, Artificial neural network modeling of dyestuff solubility in supercritical CO₂ is gradually gaining importance due to the sheer volume of its applications in modeling clarification [9], removal, solubility of novel dyes and derivatives [10,11], and commercial-grade dye purification. Tabaraki et al., [12,13] and Khazaiepour et al., [14] have studied artificial and wavelet neural network modeling of dyestuff solubility in supercritical CO₂ with different techniques on homogenous (mono class) dye samples yielding deviant results from each other. On the other hand, previous research works [3,15–20] involving the use of numerous semi-empirical models for modeling their experimental solubility data have inundated the research on dye solubility modeling with ambiguity.

Grey relational analysis by D. Julong [21] is a proven optimization method to determine the best parameter settings for identifying the maximum desired output. Additionally, Grey approach has been employed extensively by various studies for problems associated with complicated interrelationships among performance characteristics combined with uncertain, irregular, incomplete, and disorganized data. There are no restrictions on the number of variables employed for modeling a phenomenon using artificial neural networks. Hence, Grey relational analysis could be employed for studying complex models such as this to establish the optimum regime for parameter (controlled variable) setting during (pilot) process execution for the maximum desired output and minimum resource loss.

The prime objective of this study is to (1) employ artificial neural network for modeling the solubility of three different classes of dyes in supercritical CO₂ with ethanol as the co-solvent. (2) Investigate the solubility modeling efficiency of different semi-empirical equations on the prepared data sample. (3) Employ the use of Grey relational analysis to identify the regime of the controllable real-time parameters for maximum dye solubility in supercritical CO₂. (4) To perform a comparative analysis of parametric variation and its effect on dye solubility as observed from

previously studied models and theoretical fluid phase equilibria for drawing a clear conclusion.
 (5) Present a hypothesis for selective dye-extraction from multi-dye mixtures based on retrograde solubility interference.

3 Materials and Methods

3.1 Data Acquisition and parametric description

A total of 250 data points pertaining to the solubility of three different classes of dyes (eight dyes in total) were mined and curated from the literature. The experimental solubility data and the structures of the dyes required for the present study were procured from the literature cited in Table 3-2: Structures of the studied dyes.. Three anthraquinone dyes, four azo dyes, and one quinoline dye were strategically selected to introduce qualitative diversity for accurate modeling. Temperature, pressure, Total surface area, critical pressure and temperature, and molecular weight were the mined/computed attributes for the corresponding dye. The total polar surface area of the dyes was calculated using Peter Ertl et al., method [22]. The critical properties of the solutes were obtained from literature survey and from the NIST database [23]. The entire data set was normalized between 0 and 1 using the equation (1) for artificial neural network simulation. The range of the selected parameters are tabulated in Table 3-1.

$$\text{Normalized value} = \frac{X_{\text{actual}} - X_{\text{min}}}{X_{\text{max}} - X_{\text{min}}} \quad (1)$$

Parameter	Range
Temperature (K)	308 - 423.15
Pressure (MPa)	4.2 - 35.5
Density (kg/m ³)	214 - 978.782
Critical Temperature (K)	348.4 - 1361
Critical Pressure (MPa)	1.68241 - 12.46
Molecular weight (g/mol)	240.21 - 639.41
Total Polar Surface Area (Å)	67.26 - 210.53
Dye solubility mole fraction	0.000000194 - 0.000136

Table 3-1: Range of the parameters utilized for modeling.


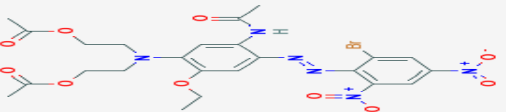
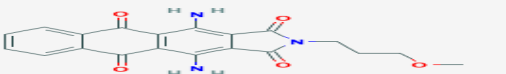

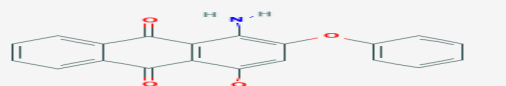
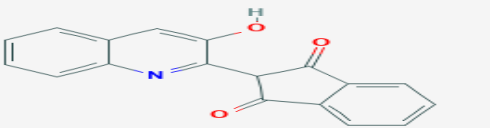
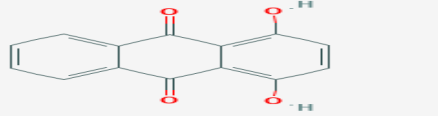
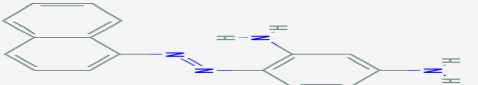
Sl No	Dye	Structure	References
1	4-(N, N-diethylamino)-4'-Nitroazobenzene		[24]
2	Disperse Blue 79		[17,25]
3	Disperse Blue 60		[26]
4	Disperse Orange 3		[25]
5	Disperse red 60		[26,27]
6	Disperse Yellow 54		[28]
7	Quinizarin		[17]
8	Solvent Brown 1		[25]

Table 3-2: Structures of the studied dyes.

3.2 Feed Forward Backpropagation-Artificial Neural Network (FFB-ANN) Architecture and Modeling

A 64-bit, 8Gb RAM workstation with a 1.99 GHz processor, was used for all computation. MATLAB 2019b software from <https://in.mathworks.com/> was used for building the tri-layer neural network architecture and its simulation trials. The architecture of the constructed neural network comprised of the first layer termed as the input layer with of seven nodes corresponding to the seven input parameters. The second layer comprised of a range of three to eight nodes with single node increment for heuristic computation during each of the six trial simulations. The third layer was comprised of a single output node corresponding to the solubility of the dye. A tangent-sigmoid (tansig) transfer function was used for the hidden layer nodes, and a linear function was used for the output layer node. A gradient descent with momentum weight and bias learning function (LearnGdm) along with backpropagation based Levenberg-Marquardt algorithm (trainlm) was employed for calculation and optimization of layer to layer and node to node weights for all simulation trials. Mean squared error was selected as the performance function, and 2000 epochs was the maximum set for each simulation. The entire data set was divided into the ratio of 6:2:2 (60%, 20%, 20%) for training, validation, and testing sets, respectively [29], and this ratio was fixed for each trial run. Continuous simulations were reinitiated until the training accuracy reached the maximum possible value, and convergence of weight optimization was reached (weights and bias do not change with additional training rounds after convergence). Care was taken to avoid overfitting (validation and testing accuracy > training accuracy) of the data.

3.2.1 Statistical Evaluation of the Artificial neural network (FFB-ANN) Model

Statistical evaluation of the model was performed using the Microsoft excel 2019 and GraphPad prism software. Nash–Sutcliffe model efficiency coefficient (**N-S**) was computed for the predicted solubility for all the simulation trials using the equation (2).

$$N - S = 1 - \frac{\sum_{i=1}^n (y_i^{\text{exp}} - y_i^{\text{pred}})^2}{\sum_{i=1}^n (y_i^{\text{exp}} - \bar{y})^2} \quad (2)$$

Additionally, mean absolute error (MAE), mean square error (MSE), root mean square error (RMSE), and coefficient of correlation (R^2) were also computed using the equations (3,4,5).

$$\text{Mean Absolute Error} = \frac{1}{n} \sum_{i=1}^n |(y_i^{\text{exp}} - y_i^{\text{pred}})| \quad (3)$$

$$\text{Mean Square Error} = \frac{1}{n} \sum_{i=1}^n (y_i^{\text{exp}} - y_i^{\text{pred}})^2 \quad (4)$$

$$\text{Root Mean Square Error} = \sqrt{\frac{1}{n} \sum_{i=1}^n (y_i^{\text{exp}} - y_i^{\text{pred}})^2} \quad (5)$$

3.3 Assessment of relative variable importance Pearson product-moment correlation analysis

Pearson product-moment correlation coefficient ($r_{x,y}$) was computed to estimate the extent and nature of inter variable correlation using the equation (6).

$$r_{x,y} = \frac{\text{COV}(x,y)}{\sigma_x \sigma_y} = \frac{E((x - \mu_x)(y - \mu_y))}{\sigma_x \sigma_y} \quad (6)$$

Where σ_x, σ_y are the standard deviations of the two variables (x, y), and $\text{COV}(x,y)$ is the covariance of the two variables. Pearson product-moment correlation coefficient of any two variables is defined as the ratio of covariance of the two variables to the product of standard deviations of the two variables. The range of $r_{x,y}$ is from -1 to 1. An absolute value of 1 corresponds to a perfect correlation between the variables; likewise, a value of 0 corresponds to no correlation. The coefficient sign indicates the nature/quality of the relationship between the variables and corresponds to the positive and negative correlation between the variables [30]. A heat-map representation of the results was plotted, and the relative importance of the variables was assessed.

3.4 Analysis of Density-Based Semi-Empirical Models

In this study, twelve different density-based semi-empirical models were selected for assessing their efficiency in modeling the solubility of the prepared sample of dyes in supercritical CO₂. Modified Adachi-lu model by Sparks et al., Bian et al., Sung and Shim, Chrastil, Jafari Nejad et al., Sodeifian et al., Keshmiri, Garlapati and Madras, Jouyban et al., Khansary, Kumar, and Johnston (K-J) and Méndez-Santiago and Teja (MST) models were studied for their efficiency in modeling the sample of solubility data used in this study. The equations of the studied models are tabulated in the Table 3-3. Solver add-in from Excel 2019 was used to perform regression analysis and for the computation of model constants with mean absolute error as the minimized objective function. Statistical analysis was performed on the different model predictions by the computation and analysis of mean absolute error (MAE), mean square error (MSE), root mean square error (RMSE), and coefficient of correlation (R^2) using the equations (3,4,5).

Sl No	Model	Equation	References
1	Chrastil	$\ln(y) = A + \frac{B}{T} + C(\ln(\rho))$	[31]
2	Kumar-Johnston	$\ln(y) = A + B(\rho) + \frac{C}{T}$	[32]
3	Jouyban	$\ln(y) = A + B(P) + C(P^2) + D(PT) + E\left(\frac{T}{P}\right) + F(\ln(\rho))$	[33]
4	Mendez-Teja	$T\ln(y\rho) = A + B(\rho) + C(T)$	[34]
5	Sung and Shim	$\ln(y) = \left(A + \frac{B}{T}\right)(\ln(\rho)) + \frac{C}{T} + D$	[26]
6	Garlapati-Madras	$\ln(y) = A + (B + C(\rho))(\ln(\rho)) + \frac{D}{T} + E(\ln(\rho T))$	[35]
7	Jafari-Nejad	$\ln(y) = A + B(p^2) + C(T^2) + D(\ln(\rho))$	[36]
8	Keshmiri	$\ln(y) = A + \frac{B}{T} + C(P^2) + \left(D + \frac{E}{T}\right)(\ln(\rho))$	[37]
9	Khansary	$\ln(y) = \frac{A}{T} + B(P) + C\left(\frac{p^2}{T}\right) + (D + E(p))(\ln(\rho))$	[38]
10	Bian	$\ln(y) = A + \frac{B}{T} + \frac{C(\rho)}{T} + (D + E(\rho))(\ln(\rho))$	[39]
11	Sodefian	$\ln(y) = A + B\left(\frac{P^2}{T}\right) + C(\ln(\rho T)) + D(\rho(\ln(\rho))) + E(P(\ln(T))) + F\left(\frac{\ln(\rho)}{T}\right)$	[40]
12	Adachi-Lu	$y = \rho^{A+B\rho+C(\rho^2)} \exp\left(\frac{a}{T} + b\right)$	[41]

Table 3-3: List of the semi-empirical models investigated for dye solubility modeling.\

3.5 Grey Relational Analysis

Grey relational analysis was applied to the procured data for establishing the generalized optimum regime of parameter settings leading to maximum dye solubility in supercritical CO₂. FFB-ANN predicted solubility and corresponding experimental solubility were simultaneously selected as the performance measures. The entire data was initially normalized for the higher-the-better performance characteristic using equation (7).

$$x_i^*(k) = \frac{x_i^0(k) - \min(x_i^0(k))}{\max(x_i^0(k)) - \min(x_i^0(k))} \quad (7)$$

Further, the grey relational coefficient $\xi_i(i)$ for the k^{th} performance characteristics in the i^{th} experiment is computed using equation (8).

$$\xi_i(i) = \frac{\Delta_{\min} - \zeta\Delta_{\max}}{\Delta_{oi}(k) - \zeta\Delta_{\max}} \quad (8)$$

The deviation between reference and comparability sequences is represented using Δ_{oi} where, $\Delta_{oi} = \|x_o^*(k) - x_i^*(k)\|$; $0 < \xi_i(i) < 1$; $\Delta_{\min} = \min_{vj \in i} \min_{vk} \|x_o^*(k) - x_i^*(k)\|$ and $\Delta_{\max} = \max_{vj \in i} \max_{vk} \|x_o^*(k) - x_i^*(k)\|$. The reference equation is denoted by $x_o^*(k)$ and the comparability sequence is denoted by $x_i^*(k)$. ζ is the distinguishing coefficient defined in the range of $0 \leq \zeta \leq 1$. The value of ζ is generally taken as 0.5; hence, the value $\zeta = 0.5$ was used. Grey relational grade was computed by calculating the average of the grey relational coefficients using equation (9) [42].

$$\gamma_i = \frac{1}{n} \sum_{k=1}^n \xi_i(i) \quad (9)$$

The computed grey relational grades pertaining to each experiment were ranked in the order (max (grey relational grade) = 1st rank). The optimum settings for the control parameters were determined by the range of the variable magnitudes corresponding to the top five ranks.

4 Results and Discussion

4.1 Optimization of the ANN-FFBP architecture and performance assessment

In this work, the input variables, temperature (308 K - 423.15 K), pressure (4.2MPa - 35.5 MPa), density (214 Kgm⁻³ - 978.782 Kgm⁻³), critical temperature (348.4 K - 1361 K), critical pressure (1.68241 MPa - 12.46 MPa), molecular weight (240.21 Kgmol⁻¹ - 639.41 Kgmol⁻¹) and total polar surface area (67.26 Å- 210.53 Å) utilized in this sample were used for the prediction of dye solubility in supercritical CO₂ using ANN-FFB simulations. Empirical equations are available for identifying the optimum hidden neurons, but these equations are problem-specific, and post-optimization is an efficient option. Hence, the number of neurons in the hidden layer was optimized through the trial-and-error method after data preparation [43]. Primarily, A simple one-tailed test with a 95% confidence interval was performed for the comparison of means of the experimental and predicted data sample. Further, additional statistical parameters like MAE, MSE, RMSE, N-S coefficient were used as the screening parameter for the selection of the best ANN-FFB architecture. FFB-ANN predicted v/s experimental data parity plot along with those obtained from MATLAB, are illustrated in Figure 4-1 and Figure 4-2.

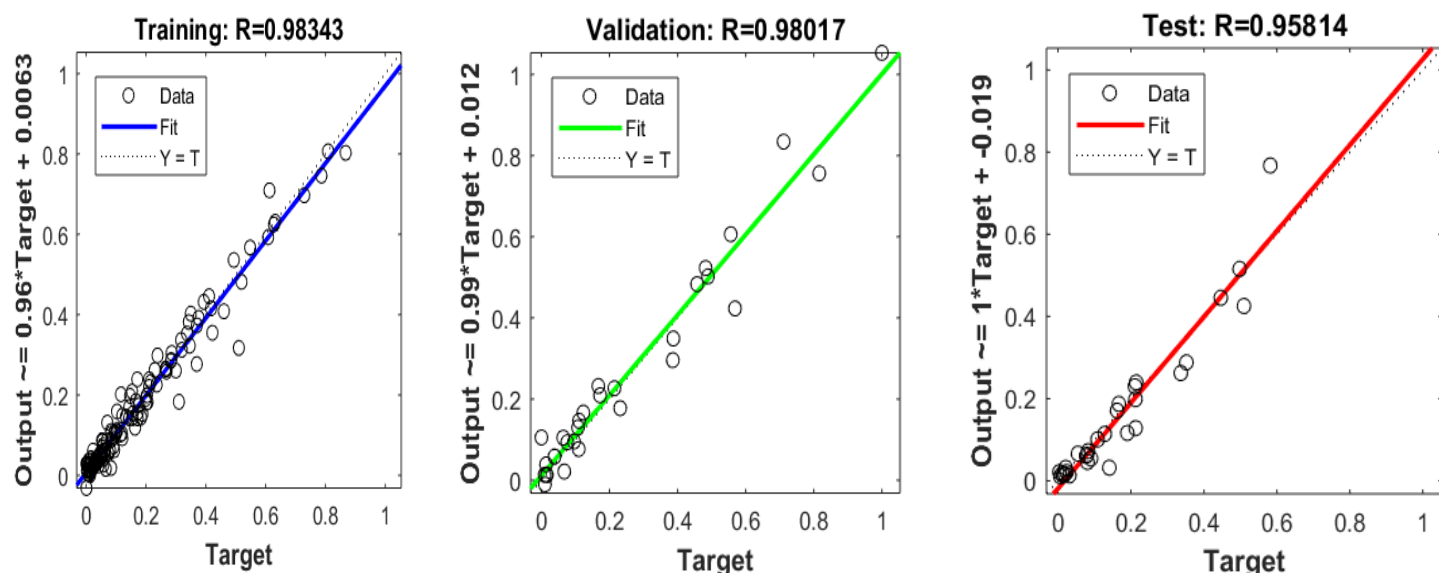


Figure 4-1: Individual regression plots pertaining to the training, validation and testing of the sample data for the ANN simulation of the (7-7-1) architecture.

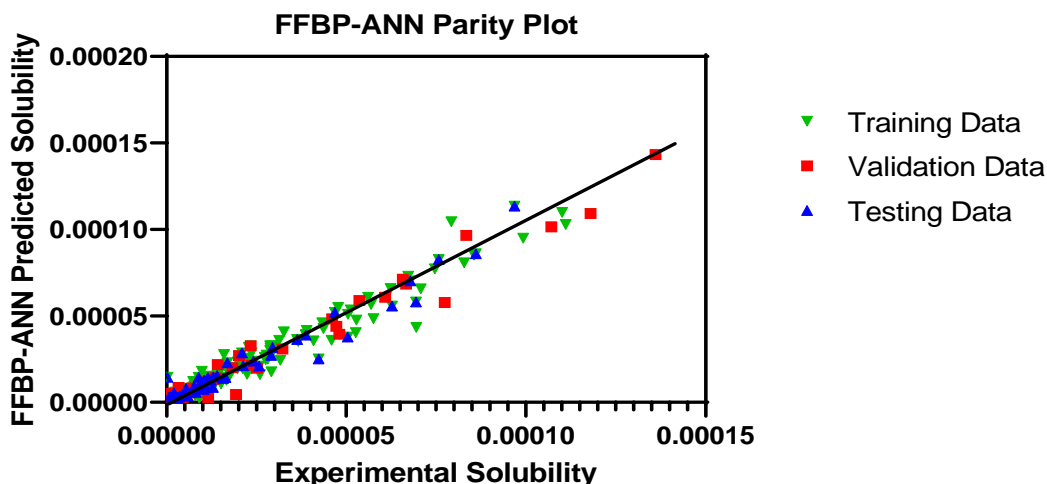


Figure 4-2: Consolidated experimental v/s FFBP-ANN predicted data parity plot of the (7-7-1) architecture ANN simulation.

The architecture [7-7-1] was found to have the least error of prediction (MSE, MAE, RMSE) and the highest correlation (R^2 and N-S coefficient). Although, an eight and seven hidden layer neuron architecture was reported twice by Tabaraki et al. [12,13] as the best for prediction of solubility of homogeneously separate samples of azo and anthraquinone dyes in SCCO_2 . The results from this study corroborate that found by Aminian (2017) for a qualitatively diverse set of non-dye solutes and sufficiently proves that a seven-neuron architecture is optimum for modeling qualitatively diverse samples [44]. The values of the learning rate and learning momentum are insignificant as they only relate to the time of convergence (which is anywhere between 1-10 minutes) and is

unrelated to the predictive ability of the model. The magnitude of the computed statistical parameters for the neural network architectures are mentioned in Table 4-1.

Number of Hidden Neurons	Mean Absolute Error	Mean Square Error	Root Mean Square Error	Nash-Sutcliffe Coefficient	R ²
3	0.032156734	0.002206362	0.046971933	0.940933336	0.9453
4	0.038522305	0.002983261	0.054619237	0.916034027	0.9265
5	0.027625966	0.001720562	0.041479661	0.954218723	0.9579
6	0.218200168	0.324921136	0.57001854	-0.400668281	0.0007078
7	0.02641665	0.001665037	0.040804865	0.958862568	0.9832
8	0.038094406	0.022457094	0.149856912	0.642780364	0.6456

Table 4-1: Hidden layer optimization trials and their corresponding statistical indices

It is important to note that the value of mean absolute error, mean square error, root mean square error, and Nash-Sutcliffe coefficient obtained in this study for the [7-7-1] architecture is 0.026, 0.0016, 0.04 and 0.9588 respectively. These error indices are significantly better than those reported twice by Tabaraki et al. [12,13] for dyestuff solubility modeling in SCCO₂. Although Khazaiepour et al., [14] have reported lower and better error indices in testing data prediction for dyestuff solubility modeling in SCCO₂, The indices reported by them is for a qualitatively homogenous sample of three azo dyes with eight testing data points (n= 15% of the total 48 data points = eight testing data points). The present study has investigated a qualitatively heterogenous dye sample of a total of 250 data points with 20% testing data (n= 40 points), making this a pervasive, properly fit, robust model. According to Jha et al., the pioneers in solubility modeling using ANN, a ubiquitous, properly fit, robust model should undergo training with consistent accuracy, without the influence of the initial weight and bias settings. Additionally, such a model should be versatile in predicting the solubility of a broader spectrum of solutes (this case dyes). An overly fit model (e.g., $R^2 = 0.9999$; $R^2_{\text{train}} < R^2_{\text{validation}}, R^2_{\text{testing}}$), when reused/expanded, would require more time for convergence, additional training rounds and would not accurately predict the solubility of solute classes that were not considered for training [45].

4.2 Assessment of relative variable importance

Assessment of variable importance was primarily performed using the simulation neural network 1.0 software obtained from Prof. Montañó [46]. But the slope of means method (numeric sensitivity analysis) is inefficient in calculating the relative variable importance as it does not consider the effect of retrograde solubility interference, region-specific calculations are tedious and time-consuming and are not supported by the software. Likewise, Garson's method [47] has been reported to be relatively less efficient compared to numeric sensitivity analysis by Montañó et al., [46]. Hence, Pearson's product-moment correlation coefficient was computed for the quantitative measurement of the relationship strengths between the input variables and dye solubility. The values of the computed coefficients are illustrated in the form of a heat map in Figure 4-3 .

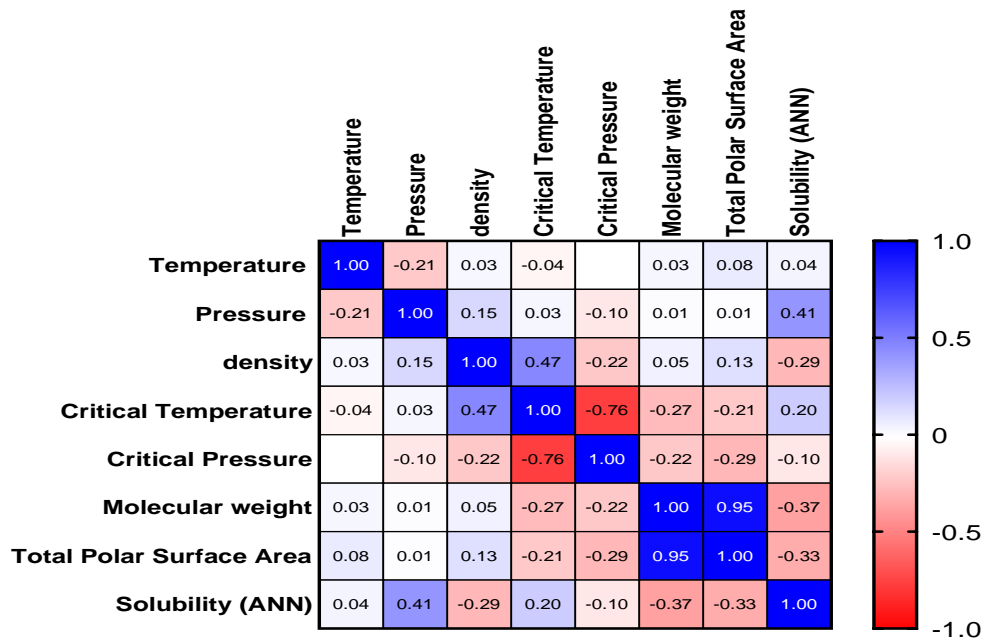


Figure 4-3: Heat map chart of the Pearson product moment correlation analysis performed on the input and output variables of the FFBP-ANN model.

The analysis of the heat-map reveals that pressure has the highest positive correlation (0.41) with solubility. This may be due to the fact that an increase in pressure causes a proportional increase in density, leading to increased solubility. But this behavior is limited to a threshold, beyond which an increase in pressure causes an increase in fluid viscosity, contributing to decreased solubility. This behavior has been reported by Suryawanshi et al [48]. Khazaiepour et al, [14] in their studies have included acentric factor for ANN modeling. For the computation of the acentric factor, vapor pressure data at the reference temperature is required, whereas, for the calculation of the total polar surface area, the molecular structure of the solute is sufficient. Since the acentric factor and TPSA are interdependent, TPSA was used as an input parameter for modeling in this study, as it is relatively easy to compute (future model expansion propagates smoothly without any hassles regarding uncomputable/missing identifiers). Temperature as an input variable was found to have a low correlation coefficient of 0.04 with solubility, indicating that there is retrograde solubility interference at play [49]. Studies conducted by Ongkasin et al., on cefuroxime axetil solubility in supercritical CO₂ report that at isobaric conditions, an increase in temperature results in a decrease in density and solubility in the retrograde zone ($(\partial(\ln(y))/\partial T)_P < 0; \forall P_L < P_{\text{Solute}} < P_U$), (where supercritical CO₂ density effect is predominant) But, at pressures lower and nearer to the lowest pressure limit of the retrograde zone along with pressures higher than the upper cross-over pressure ($(\partial(\ln(y))/\partial T)_P > 0; \forall 0 < P_{\text{Solute}} < P_L$), the effect of solute vapor pressure becomes predominant wherein an increase in temperature results in increased solubility [50]. Further, Density was found to have a negative correlation with solubility with a coefficient of -0.29. Hence, we can infer two aspects. First, that most of the solubility data analyzed in this study have been recorded in the retrograde zone (graphical analysis of select isotherm plots Figure 4-6 indicates an absence of either upper or lower crossover pressure) where there is a predominance of the

supercritical CO₂ density effect (since density was found to be “generally” decreased ($r_{\rho,y} = -0.29$) with increased temperature ($r_{T,y} = 0.04$)). Second, the correlation analysis sufficiently validates the generalized robustness of the proposed ANN model in this study as it relates to supercritical phase equilibria. Furthermore, critical pressure, total polar surface area and molecular weight was found to have a negative correlation with dye solubility with values of -0.1, -0.33 and -0.37 respectively. Previous studies by Aminian et al., and Madras et al., have also reported that an increase in molecular weight is related to decreased solute solubility in supercritical CO₂ [44,51] corroborating the negative correlation found between molecular weight and dye solubility in the present study.

4.3 Analysis of Density-Based Semi-Empirical Models

Various density-based semi-empirical models were investigated for their efficiency in modeling solubility of the prepared sample data. Among the models investigated, the Mendez-Teja model could model the solubility of the investigated sample with the highest statistical desirability and agreement. The root mean square error and mean absolute error were computed to be 0.094 and 0.0088, respectively. Further, a $T\ln(P_y)-C(T)$ v/s density plot for the Mendez-Teja model produced a straight trendline with relatively fewer outliers. Mendez-Teja, in their proposed model [34], elucidate the manifestation of % co-solvent as parallel trendlines in the $T\ln(P_y)-C(T)$ v/s density plot. The $T\ln(P_y)-C(T)$ v/s density plot is illustrated in Figure 4-4.

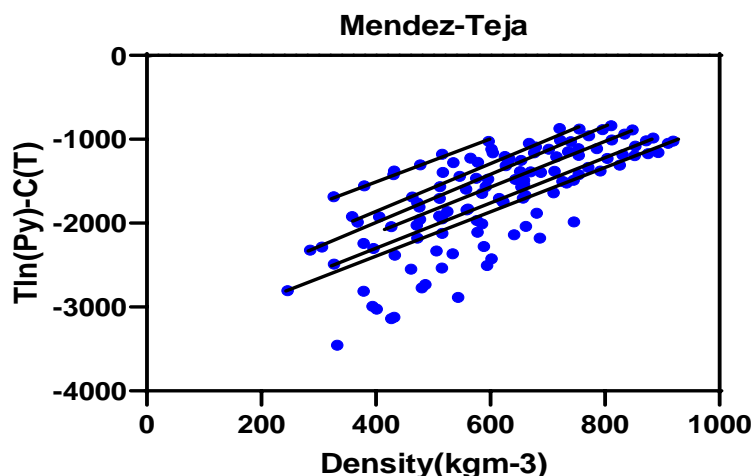


Figure 4-4: Solubility of the investigated dye sample in supercritical carbon dioxide with ethanol as the cosolvent as a function of carbon dioxide density based on the Mendez-Teja model. The trendlines depict the various dye-specific quantities of the cosolvent used during the experiments.

A total of six such trendlines corresponding to different quantities of co-solvent were observed in the plotted graphs in the present investigation. In the present study, ethanol was fixed as the co-solvent used during experimental supercritical CO₂ dye extraction studies. But the quantities (% v/v) of ethanol used during SC-CO₂ extraction were not available in the literature; hence % co-solvent was not used as a parameter during modeling. The modified Adachi-lu model was assessed as the second best with root mean square error and mean absolute error of 0.81 and 0.66, respectively. The generalized reduced gradient nonlinear regression method was employed to

obtain the coefficients of the investigated models. The coefficients and the computed statistical results of the models are tabulated in Table 4-2 and Table 4-3, respectively.

Sl. No	Model	Constants					
		A0	A1	A2	A3	A4	A5
1	Sodeifian	0.00000000	0.00122297	0.31395470	1.06949312	0.00000000	0.00000000
2	Chrastil	0.66979881	0.01002547	0.00000000	-	-	-
3	Mendez-Teja	-0.00001000	-0.00001000	0.00050000	-	-	-
4	Kumar-Johnston	0.00000100	0.02500000	-0.00100000	-	-	-
5	Garlapati-Madras	0.00000000	0.00117374	0.41996382	0.00000000	0.31953855	-
6	Bian	0.00100000	-0.00125600	0.00000000	0.34070671	8.70164889	-
7	Jouyban	0.00650000	0.10000000	0.00332250	-0.85200000	0.33256800	0.66979358
8	Adachi-Lou	0.00650004	0.10000724	0.00332251	0.00000000	0.00000000	-
9	Sung-Shim	0.66938901	0.00137131	-0.00002000	-0.10000000	-	-
10	Jafari Nejad	0.01250000	0.00524500	0.50000000	0.77142091	-	-
11	Keshmiri	-0.10000000	0.00000000	0.00069883	0.66946426	0.00137151	-
12	Khansary	0.00000000	-0.98000000	0.00000000	0.77142067	0.00001372	-

Table 4-2: List of coefficients computed by regression for the studied semi empirical models.

Sl. No	Model	Mean Absolute Error	Mean Square Error	Root Mean Square Error
1	Sodeifian	1.262810800	2.393379750	1.547055186
2	Chrastil	1.662136793	4.443887237	2.108052949
3	Mendez-Teja**	0.076245542	0.008855853	0.094105541
4	Kumar-Johnston	2.482661146	8.209164473	2.865163952
5	Garlapati-Madras	1.282402424	2.417726482	1.554904010
6	Bian	1.264790149	2.549767198	1.596799047
7	Jouyban	1.685864316	4.584924683	2.141243723
8	Adachi-Lou	0.789928909	0.663590305	0.814610523
9	Sung-Shim	1.675118977	4.149285530	2.036979512
10	Jafari Nejad	1.681321920	4.379746081	2.092784289
11	Keshmiri	1.676286058	4.158139919	2.039151765
12	Khansary	1.663022109	3.889074271	1.972073597

Table 4-3: Statistical indices pertaining to the analyzed semi-empirical models.

4.4 Optimum parameter settings and estimation of crossover pressure.

The performed Grey relational analysis predicted optimum values of the adjustable experimental parameters during SCCO₂ extraction of the investigated dyes in the sample. The range of predicted optimum parameter values of temperature and pressure with higher the better solubility characteristics corresponding to the top five ranks are 353.2 K to 373.2 K and 25 MPa to 26.1 MPa, respectively. These are general settings that yield maximum dye solubility and are not dye-specific. The dye-specific range of parameters and the resultant dye-specific solubility from the experimental data (illustrated in Figure 4-5) was used to better understand the overview of their effect on solubility.

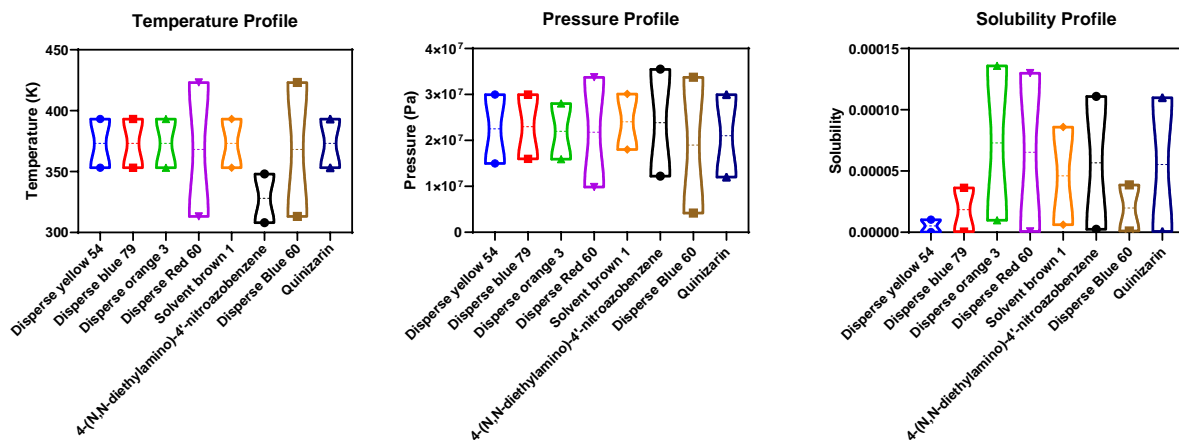


Figure 4-5: Parameter profile violin plots illustrating the dye specific ranges of temperature, pressure and solubility.

The cross-over pressures of the individual dyes were estimated from solubility v/s pressure isotherm plots of individual dyes, and the obtained data is tabulated in Table 4-4. Thermodynamically, the crossover region of a solute in supercritical CO₂ is estimated by using the equation criteria (10).

$$(\partial(\ln(y))/\partial T)_P = 0 \text{ at } P = P_L, P = P_U. \quad (10)$$

Three anthraquinone dyes, Quinizarin, Disperse Blue 60 and Disperse Red 60, displayed a generalized crossover pressure region ranging from 16 MPa to 24 MPa. Likewise, three azo dyes, Disperse Blue 79, Disperse Orange 3, and 4-(N, N-Diethylamino)-4'-Nitroazobenzene displayed a generalized crossover region ranging from 9 MPa to 20 MPa. The crossover region of Solvent Brown 1 (Azo class) dye could not be estimated from the range of the recorded data. Finally, the generalized crossover pressure region of Disperse Yellow 54 (Quinoline class) dye ranged from 15 MPa to 20 MPa. The isotherms are depicted in Figure 4-6.

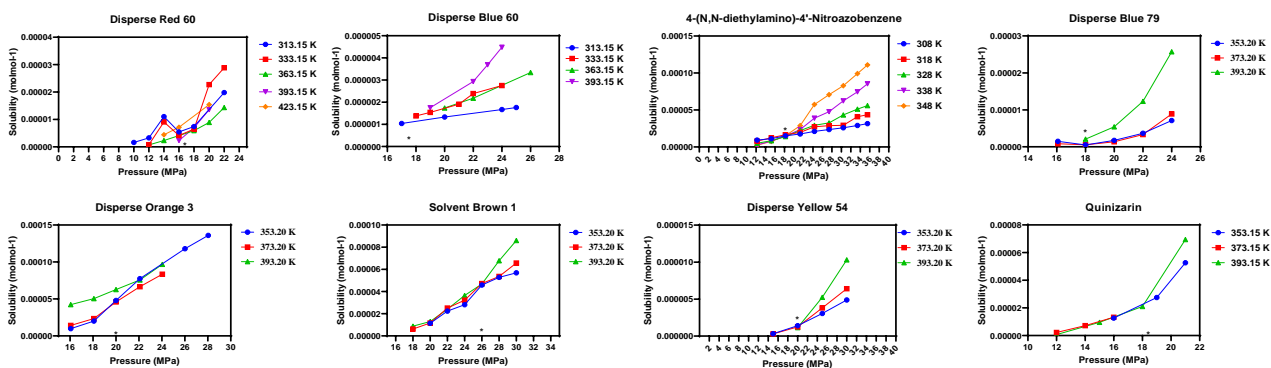


Figure 4-6: Dye specific isotherm plots that illustrate crossover points (*).

Experimental studies conducted on Phenanthrene deposition/recrystallization by Esmaeilzadeh et al., in a tri-solute system report that Phenanthrene can be selectively purified from a tri-solute mixture by fixing the pressure (isobaric) in the cross-over region of other constituent solutes and by gradually increasing the temperature [52]. Likewise, upon fixing the pressure between 9 MPa (P_L (Azo)) to 16 MPa (P_L (Anthraquinone)) (empirically determined error factor should be considered if any solute-solute interactions cause changes in the crossover region) and by gradually increasing the temperature (353.2 K to 373.2 K), Anthraquinone and Azo dyes could be selectively purified from their mixtures (Anthraquinone + Azo) as only one dye solute class (Anthraquinones in this case) would be relatively more soluble in SC-CO₂ at $((\partial(\ln(y)))/\partial T)_P > 0$; $\forall 0 < P_{\text{Anthraquinone}} < P_L$). Further, for sustainable single solute dye extraction in SC-CO₂, isobaric increase in temperature (353.2 K to 373.2 K) while the pressure is fixed at $((\partial(\ln(y)))/\partial T)_P > 0$; $\forall 0 < P_{\text{Solute}} < P_L$) would yield maximum solubility with minimum resource consumption. The identified retrograde zones of the individual dyes are tabulated in Table 4-4.

Dye	Dye Class	Lower Crossover Pressure	Upper Crossover Pressure
4-(N, N-Diethylamino)-4'-Nitroazobenzene	Single Azo Class	9-10	18
Disperse Blue 79	Single Azo Class	18	22
Disperse Blue 60	Anthraquinones	21	24
Disperse Orange 3	Single Azo Class	14-15	19.5
Disperse Red 60	Anthraquinones	16	18
Disperse Yellow 54	Quinoline Class	15	20
Quinizarin	Anthraquinone	17	18.3
Solvent Brown 1	Single Azo Class	Unclear	Unclear

Table 4-4: List of Dyes, their classes and their respective crossover pressures.

5 Funding

This research did not receive any specific grant from funding agencies in the public, commercial, or not-for-profit sectors.

6 Acknowledgements

The authors would like to acknowledge the support from Dr Ganapathi Shankarling, Department of Dyestuff Technology, Institute of Chemical Technology, Mumbai, Maharashtra, India.

7 Conclusions

Based on the outcomes of the present investigations, the following conclusions were drawn

1. A generalized, properly fit, robust feed-forward artificial neural network model was developed using a backpropagation based Levenberg-Marquardt algorithm on a qualitatively diverse sample of three anthraquinone dyes, four azo dyes and one quinoline dye for modeling their solubility in supercritical carbon-di-oxide with ethanol as the fixed co-solvent. The optimized neural network architecture was realized to be composed of 7 hidden neurons (7-7-1). The mean absolute error, mean square error, root mean square error and Nash-Sutcliffe coefficient was computed to be 0.026, 0.0016, 0.04 and 0.9588,

respectively. The coefficient of determination (R^2) for training, validation, and testing were computed to be 0.983, 0.980, and 0.958, respectively.

2. Among the twelve investigated semi-empirical models, the Mendez-Teja model was found to be the best for predicting solubility in supercritical carbon-di-oxide for the prepared sample of dyes. The root mean square error and mean absolute error were computed to be 0.094 and 0.0088, respectively.
3. Grey relational analysis with higher the better dye solubility as the performance characteristic was employed to identify the optimum regime of parameter settings for maximized dye solubility. Retrograde solubility interference was observed, and the individual (dye-specific) crossover pressure range was identified. Selective purification of dyes in a multi-solute system using supercritical carbon-di-oxide extraction has been discussed based on the identified parameter regimes.

8 References

- [1] H. Kamali, H.S. Ghaziaskar, Pressurized hot water extraction of benzoic acid and phthalic anhydride from petrochemical wastes using a modified supercritical fluid extractor and a central composite design for optimization, *J. Supercrit. Fluids*. 54 (2010) 16–21. doi:10.1016/j.supflu.2010.04.002.
- [2] A. Natolino, C. Da Porto, Supercritical carbon dioxide extraction of pomegranate (*Punica granatum* L.) seed oil: Kinetic modelling and solubility evaluation, *J. Supercrit. Fluids*. 151 (2019) 30–39. doi:10.1016/j.supflu.2019.05.002.
- [3] J. Yan, L.J. Zheng, B. Du, Y.F. Qian, F. Ye, Dye solubility in supercritical carbon dioxide fluid, *Therm. Sci.* 19 (2015) 1311–1315. doi:10.2298/TSCI1504311Y.
- [4] K.C. Pitchaiah, K. Sujatha, J. Deepitha, S. Ghosh, N. Sivaraman, Recovery of uranium and plutonium from pyrochemical salt matrix using supercritical fluid extraction, *J. Supercrit. Fluids*. 147 (2019) 194–204. doi:10.1016/j.supflu.2018.10.015.
- [5] F.P. Lucien, N.R. Foster, Solubilities of solid mixtures in supercritical carbon dioxide: A review, *J. Supercrit. Fluids*. 17 (2000) 111–134. doi:10.1016/S0896-8446(99)00048-0.
- [6] F. Gharagheizi, A. Eslamimanesh, A.H. Mohammadi, D. Richon, Representation/Prediction of solubilities of pure compounds in water using artificial neural network-group contribution method, *J. Chem. Eng. Data*. 56 (2011) 720–726. doi:10.1021/je101061t.
- [7] I. Rivals, L. Personnaz, BLACK-BOX MODELING WITH STATE-SPACE NEURAL NETWORKS, 1996.
- [8] J. Schmidhuber, Deep Learning in neural networks: An overview, *Neural Networks*. 61 (2015) 85–117. doi:10.1016/j.neunet.2014.09.003.
- [9] S. Foorginezhad, M.Z.-D.A. WATER, undefined 2019, Preparation of low-cost ceramic membranes using Persian natural clay and their application for dye clarification, Deswater.Com. (n.d.).

https://www.deswater.com/DWT_abstracts/vol_145/145_2019_378.pdf (accessed March 7, 2020).

- [10] G.S. Shankarling, K.J. Jarag, Laser dyes, *Resonance*. 15 (2010) 804–818. doi:10.1007/s12045-010-0090-9.
- [11] U.N. Yadav, G.S. Shankarling, Synergistic effect of ultrasound and deep eutectic solvent choline chloride-urea as versatile catalyst for rapid synthesis of β -functionalized ketonic derivatives, *J. Mol. Liq.* 195 (2014) 188–193. doi:10.1016/j.molliq.2014.02.016.
- [12] R. Tabaraki, T. Khayamian, A.A. Ensafi, Wavelet neural network modeling in QSPR for prediction of solubility of 25 anthraquinone dyes at different temperatures and pressures in supercritical carbon dioxide, *J. Mol. Graph. Model.* 25 (2006) 46–54. doi:10.1016/j.jmglm.2005.10.012.
- [13] R. Tabaraki, T. Khayamian, A.A. Ensafi, Solubility prediction of 21 azo dyes in supercritical carbon dioxide using wavelet neural network, *Dye. Pigment.* 73 (2007) 230–238. doi:10.1016/j.dyepig.2005.12.003.
- [14] A. Khazaiepour, M. Soleimani, S. Salahi, Solubility prediction of disperse dyes in supercritical carbon dioxide and ethanol as co-solvent using neural network, *Chinese J. Chem. Eng.* 24 (2016) 491–498. doi:10.1016/j.cjche.2015.11.027.
- [15] K. Mishima, K. Matsuyama, H. Ishikawa, K.I. Hayashi, S. Maeda, Measurement and correlation of solubilities of azo dyes and anthraquinone in supercritical carbon dioxide, *Fluid Phase Equilib.* 194–197 (2002) 895–904. doi:10.1016/S0378-3812(01)00720-8.
- [16] K. Tamura, T. Shinoda, Binary and ternary solubilities of disperse dyes and their blend in supercritical carbon dioxide, *Fluid Phase Equilib.* 219 (2004) 25–32. doi:10.1016/j.fluid.2004.01.009.
- [17] A. Ferri, M. Banchero, L. Manna, S. Sicardi, An experimental technique for measuring high solubilities of dyes in supercritical carbon dioxide, *J. Supercrit. Fluids.* 30 (2004) 41–49. doi:10.1016/S0896-8446(03)00114-1.
- [18] C.L. Cui, W. Shi, J.J. Long, Solubility and data correlation of a reactive disperse dye in a quaternary system of supercritical carbon dioxide with mixed cosolvents, *J. Taiwan Inst. Chem. Eng.* 91 (2018) 213–223. doi:10.1016/j.jtice.2018.06.028.
- [19] T. Funazukuri, T. Yamasaki, M. Taguchi, C.Y. Kong, Measurement of binary diffusion coefficient and solubility estimation for dyes in supercritical carbon dioxide by CIR method, *Fluid Phase Equilib.* 420 (2016) 7–13. doi:10.1016/j.fluid.2016.01.010.
- [20] E. Bach, E. Cleve, J. Schuttken, E. Schollmeyer, J.W. Rucker, Correlation of solubility data of azo disperse dyes with the dye uptake of poly(ethylene terephthalate) fibres in supercritical carbon dioxide, *Color. Technol.* 117 (2001) 13–18. doi:10.1111/j.1478-4408.2001.tb00329.x.
- [21] D. Julong, Introduction to Grey System Theory, *J. Grey Syst.* 1 (1989) 1–24.
- [22] P. Ertl, B. Rohde, P. Selzer, Fast calculation of molecular polar surface area as a sum of fragment-based contributions and its application to the prediction of drug transport

- properties, *J. Med. Chem.* 43 (2000) 3714–3717. doi:10.1021/jm000942e.
- [23] E.W. Lemmon, M.O. McLinden, and D.G. Friend, NIST Chemistry WebBook, NIST Standard Reference Database, 2017. doi:10.18434/T4D303.
- [24] J. Fasihi, Y. Yamini, F. Nourmohammadian, N. Bahramifar, Investigations on the solubilities of some disperse azo dyes in supercritical carbon dioxide, *Dye. Pigment.* 63 (2004) 161–168. doi:10.1016/j.dyepig.2004.01.007.
- [25] M. Banchero, A. Ferri, L. Manna, S. Sicardi, Solubility of disperse dyes in supercritical carbon dioxide and ethanol, *Fluid Phase Equilib.* 243 (2006) 107–114. doi:10.1016/j.fluid.2006.02.010.
- [26] H. Do Sung, J.J. Shim, Solubility of C. I. Disperse Red 60 and C. I. Disperse Blue 60 in supercritical carbon dioxide, *J. Chem. Eng. Data.* 44 (1999) 985–989. doi:10.1021/je990018t.
- [27] P. Muthukumaran, R.B. Gupta, H. Do Sung, J.J. Shim, H.K. Bae, Dye solubility in supercritical carbon dioxide. Effect of hydrogen bonding with cosolvents, *Korean J. Chem. Eng.* 16 (1999) 111–117. doi:10.1007/BF02699013.
- [28] C.C. Tsai, H. mu Lin, M.J. Lee, Solubility of disperse yellow 54 in supercritical carbon dioxide with or without cosolvent, *Fluid Phase Equilib.* 260 (2007) 287–294. doi:10.1016/j.fluid.2007.07.070.
- [29] B. Pavlić, L. Pezo, B. Marić, L.P. Tukuljac, Z. Zeković, M.B. Solarov, N. Teslić, Supercritical fluid extraction of raspberry seed oil: Experiments and modelling, *J. Supercrit. Fluids.* 157 (2020). doi:10.1016/j.supflu.2019.104687.
- [30] M.M. Mukaka, Statistics Corner: A guide to appropriate use of Correlation coefficient in medical research, *Malawi Med. J.* 24 (2012) 69–71. doi:10.1016/j.cmpb.2016.01.020.
- [31] J. Chrastil, Solubility of solids and liquids in supercritical gases, *J. Phys. Chem.* 86 (1982) 3016–3021. doi:10.1021/j100212a041.
- [32] S.K. Kumar, K.P. Johnston, Modelling the solubility of solids in supercritical fluids with density as the independent variable, *J. Supercrit. Fluids.* 1 (1988) 15–22. doi:10.1016/0896-8446(88)90005-8.
- [33] A. Jouyban, A. Fathi-Azarbayjani, M. Khoubnasabjafari, W.E. Acree Jr, Mathematical representation of the density of liquid mixtures at various temperatures using Jouyban-Acree model, 2005. <http://nopr.niscair.res.in/handle/123456789/18069> (accessed March 6, 2020).
- [34] J. Mendez-Santiago, A.S. Teja, Solubility of solids in supercritical fluids: Consistency of data and a new model for cosolvent systems, *Ind. Eng. Chem. Res.* 39 (2000) 4767–4771. doi:10.1021/ie000339u.
- [35] C. Garlapati, G. Madras, New empirical expressions to correlate solubilities of solids in supercritical carbon dioxide, *Thermochim. Acta.* 500 (2010) 123–127. doi:10.1016/j.tca.2009.12.004.

- [36] S. Jafari Nejad, H. Abolghasemi, M.A. Moosavian, M.G. Maragheh, Prediction of solute solubility in supercritical carbon dioxide: A novel semi-empirical model, *Chem. Eng. Res. Des.* 88 (2010) 893–898. doi:10.1016/j.cherd.2009.12.006.
- [37] K. Keshmiri, A. Vatanara, Y. Yamini, Development and evaluation of a new semi-empirical model for correlation of drug solubility in supercritical CO₂, *Fluid Phase Equilib.* 363 (2014) 18–26. doi:10.1016/j.fluid.2013.11.013.
- [38] M. Asgarpour Khansary, F. Amiri, A. Hosseini, A. Hallaji Sani, H. Shahbeig, Representing solute solubility in supercritical carbon dioxide: A novel empirical model, *Chem. Eng. Res. Des.* 93 (2015) 355–365. doi:10.1016/j.cherd.2014.05.004.
- [39] X.Q. Bian, Q. Zhang, Z.M. Du, J. Chen, J.N. Jaubert, A five-parameter empirical model for correlating the solubility of solid compounds in supercritical carbon dioxide, *Fluid Phase Equilib.* 411 (2016) 74–80. doi:10.1016/j.fluid.2015.12.017.
- [40] G. Sodeifian, S.M. Hazaveie, S.A. Sajadian, N. Saadati Ardestani, Determination of the Solubility of the Repaglinide Drug in Supercritical Carbon Dioxide: Experimental Data and Thermodynamic Modeling, *J. Chem. Eng. Data.* (2019). doi:10.1021/acs.jced.9b00550.
- [41] D.L. Sparks, L.A. Estévez, R. Hernandez, K. Barlow, T. French, Solubility of nonanoic (pelargonic) acid in supercritical carbon dioxide, *J. Chem. Eng. Data.* 53 (2008) 407–410. doi:10.1021/jc700465u.
- [42] S. Dharmalingam, R. Subramanian, K. Somasundara Vinoth, B. Anandavel, Optimization of tribological properties in aluminum hybrid metal matrix composites using gray-taguchi method, *J. Mater. Eng. Perform.* 20 (2011) 1457–1466. doi:10.1007/s11665-010-9800-4.
- [43] F. Gharagheizi, A. Eslamimanesh, A.H. Mohammadi, D. Richon, Artificial neural network modeling of solubilities of 21 commonly used industrial solid compounds in supercritical carbon dioxide, *Ind. Eng. Chem. Res.* 50 (2011) 221–226. doi:10.1021/ie101545g.
- [44] A. Aminian, Estimating the solubility of different solutes in supercritical CO₂ covering a wide range of operating conditions by using neural network models, *J. Supercrit. Fluids.* 125 (2017) 79–87. doi:10.1016/j.supflu.2017.02.007.
- [45] S.K. Jha, G. Madras, Neural network modeling of adsorption equilibria of mixtures in supercritical fluids, *Ind. Eng. Chem. Res.* 44 (2005) 7038–7041. doi:10.1021/ie049010p.
- [46] J.J. Montañó, A. Palmer, Numeric sensitivity analysis applied to feedforward neural networks, *Neural Comput. Appl.* 12 (2003) 119–125. doi:10.1007/s00521-003-0377-9.
- [47] G.D. Garson, Interpreting neural-network connection weights, (1991).
- [48] B. Suryawanshi, B. Mohanty, Application of an artificial neural network model for the supercritical fluid extraction of seed oil from *Argemone mexicana* (L.) seeds, *Ind. Crops Prod.* 123 (2018) 64–74. doi:10.1016/j.indcrop.2018.06.057.
- [49] N.R. Foster, G.S. Gurdial, J.S.L. Yun, K.K. Liong, K.D. Tilly, S.S.T. Ting, H. Singh, J.H. Lee, Significance of the Crossover Pressure in Solid-Supercritical Fluid Phase Equilibria, (1991) 1955–1964.

- [50] K. Ongkasin, M. Sauceau, Y. Masmoudi, J. Fages, E. Badens, Solubility of cefuroxime axetil in supercritical CO₂: Measurement and modeling, *J. Supercrit. Fluids*. 152 (2019) 104498. doi:10.1016/j.supflu.2019.03.010.
- [51] G. Madras, C. Kulkarni, J. Modak, Modeling the solubilities of fatty acids in supercritical carbon dioxide, *Fluid Phase Equilib.* 209 (2003) 207–213. doi:10.1016/S0378-3812(03)00148-1.
- [52] F. Esmailzadeh, I. Goodarznia, Supercritical Extraction of Phenanthrene in the Crossover Region, (2005) 49–51.